Available online at www.sciencedirect.com
ScienceDirect
International Journal of Heat and Mass Transfer 50 (2007) 1833–1842
International Journal of HEAT and MASS TRANSFER
www.elsevier.com/locate/ijhmt

A general implementation of the **H1** boundary condition in CFD simulations of heat transfer in swept passages

Nathan R. Rosaguti, David F. Fletcher *, Brian S. Haynes

Department of Chemical Engineering, University of Sydney, NSW 2006, Australia

Received 15 May 2006; received in revised form 4 October 2006
Available online 5 December 2006

Abstract

A methodology has been developed to study laminar flow and heat transfer behaviour in periodic non-straight passages with a heat transfer boundary condition of constant axial heat flux and constant peripheral temperature (**H1**). The technique uses Newton iteration to determine the wall temperature distribution required to satisfy the **H1** boundary condition. The methodology is validated for hydrodynamically developed and thermally developing flow, as well as for hydrodynamically and thermally developed flow in straight ducts with various cross-sections. The methodology is extended to study fully developed flow in a periodic serpentine channel, consisting of a number of bends and straight sections, with a semi-circular cross-section. The results show the existence of a non-monotonic temperature distribution along the serpentine channels which exists because increased rates of heat transfer at bends lead to reductions in the local wall temperature in order to maintain a constant axial heat flux. Hot spots within the passage cross-section, typical of the **H2** boundary condition, are removed in the **H1** case.

Keywords: **H1** thermal boundary condition; Forced convection heat transfer; CFD; Constant section ducts

1. Introduction

The growing importance of micro-scale heat exchangers for use in chemical plants of the future and electronic cooling has led to the need to understand laminar flow heat transfer in the periodic passages of heat exchangers. Whilst the specification of hydrodynamic boundary conditions is straightforward, the choice of thermal boundary conditions is more complex. The physical situation is conduction of heat from the hot channel into a substrate and subsequently to a cold channel. The relatively high thermal conductivity of many substrate materials means that axial conduction around the tube walls tends to remove local "hot spots".

Theoretical investigations mostly consider the boundary conditions of uniform wall heat flux and uniform wall temperature (the **H2** and **T** boundary conditions, respectively [1]) due to the relative ease of their implementation in numerical models – Refs. [2–7] are examples of such implementations for a variety of flow geometries. However, these boundary conditions fail to include the important role of the substrate material. The **H1** boundary condition, defined as constant axial wall heat flux and constant peripheral wall temperature, is often a more physically representative boundary condition that goes some way to including the role of the surrounding wall material without moving to a full conjugate heat transfer solution that treats multiple channels and the matrix material in detail [8].

Previous studies of the **H1** boundary condition have been limited mainly to straight ducts [1,9–14]. The compilation of Shah and London [1] provides a database of friction factors and Nusselt numbers for various geometry cross-sections, as well as a thorough explanation of thermal boundary conditions. Table 1, adapted from Shah and London [1], shows the significant differences in Nusselt numbers for fully developed laminar flow in straight ducts of selected cross-sections under the **H1**, **H2**, and **T**

* Corresponding author. Tel.: +61 2 93514147; fax: +61 2 93512854.
E-mail address: d.fletcher@usyd.edu.au (D.F. Fletcher).

0017-9310/$ - see front matter © 2006 Elsevier Ltd. All rights reserved.
doi:10.1016/j.ijheatmasstransfer.2006.10.009

Nomenclature

c_p	heat capacity [J kg^{-1} K^{-1}]
d	passage diameter [m]
d_h	hydraulic mean diameter [m]
f	Fanning friction factor [–]
h	heat transfer coefficient [W m^{-2} K^{-1}]
J	Jacobian matrix [W m^{-1} K^{-1}]
k	thermal conductivity [W m^{-1} K^{-1}]
L	serpentine half wavelength [m]
$\dot{m}$	mass flow rate [kg s^{-1}]
N	number of axial locations at which ith column of the Jacobian is evaluated [–]
Nu	Nusselt number $= hd_h/k$ [–]
P	cross-section perimeter [m]
Q_W	total heat transfer rate to the channel [W]
q''	wall heat flux per unit area [W m^{-2}]
q'	wall heat flux per unit length [W m^{-1}]
Pe	Peclet number $= Re \cdot Pr$ [–]
Pr	Prandtl number $= c_p\mu/k$ [–]
R_c	radius of curvature [m]
Re	Reynolds number $= \bar{u}_s\rho d_h/\mu$ [–]
s	axial location along the channel [m]
S	length of the channel [m]
T	temperature [K]
$\overline{T}_B$	bulk mean temperature [K]
ΔT_S	temperature rise along one period of the channel [K]
u_s	velocity in the direction of s [m s^{-1}]
v	velocity [m s^{-1}]
$w(p)$	relative dilatation of the channel at location p [–]

Greek symbols

θ	non-dimensional temperature [–]
μ	dynamic viscosity [Pa s]
ρ	fluid density [kg m^{-3}]

Subscripts

B	bulk
H1	**H1** thermal boundary condition
H2	**H2** thermal boundary condition
M	mean
P	perimeter
W	wall
x, y	(x, y) location on a cross-section

Table 1
Friction factors and Nusselt numbers for fully developed flow in ducts of various cross-sections for different boundary conditions

Cross-section	fRe	$Nu_{\mathbf{T}}$	$Nu_{\mathbf{H1}}$	$Nu_{\mathbf{H2}}$
Circular	16	3.657	4.364	4.364
Square	14.227	2.976	3.608	3.091
Semi-circular	15.767	3.323[a]	4.089	2.923

Values (except[a]) taken from [1].
[a] Taken from [23].

boundary conditions. For non-circular passages, $Nu_{\mathbf{H1}}$ is larger than $Nu_{\mathbf{H2}}$ or $Nu_{\mathbf{T}}$ [9]. Morini [10] summarised some of the research conducted into the **H1** boundary condition as applied to straight ducts with a rectangular cross-section, and considered rectangular cross-sectioned ducts with different combinations of adiabatic and heat transferring walls. Ghodoossi and Eğrican [11] extended the application of the **H1** boundary condition in small scale rectangular channels to include wall slip, a micro-scale phenomenon.

The **H1** boundary condition has also been applied to curved passages. It is well-known that laminar flows in curved passages, such as those which occur in coiled pipes, give rise to heat transfer enhancement relative to flow in straight pipes due to their characteristic secondary flows. Flow and heat transfer research into curved ducts is well summarised by Shah and Joshi [15]. These authors suggest that the influence of the wall thermal boundary condition on the Nusselt number for helical channels with non-circular cross-sections is not significant for $Pr \geqslant 0.7$. Fully developed flow and heat transfer for the **H1** boundary condition case was examined by Kalb and Seader [16] for curved channels with circular cross-sections. Bolinder and Sundén [17] summarised the literature on flow in curved channels with square cross-sections, and investigated the effect of finite pitch on flow and heat transfer behaviour in helical channels.

A common feature of the above work is that it deals with fully developed flow in straight or spiral ducts of constant cross-section – these problems are essentially two-dimensional in nature and relatively easy to solve. Once the problem becomes three-dimensional, for example if the flow is thermally and hydrodynamically developing, or if the duct cross-section is not constant, then the solution of the problem can require very large investment into purpose-built models and computer codes, and therefore the use of commercial CFD packages becomes especially attractive. Most of these packages allow simple Dirichlet ($T = T_{wall}$, a constant everywhere, corresponding to the T boundary condition) and Neumann ($q''_{wall} =$ constant everywhere, corresponding under many circumstances to the **H2** boundary condition) boundary conditions and can therefore be used straightforwardly for **T** and **H2** boundary conditions. However, the **H1** boundary condition (heat transfer rate per unit of duct length is constant but the local heat flux around the duct may vary since the peripheral wall temperature at a given axial location is constant) cannot be implemented directly.

The present work aims to fill a gap in the literature by describing a generic methodology to implement the **H1** boundary condition in a computational fluid dynamics

(CFD) code. We demonstrate the technique by solving for flow and heat transfer in a thermally developing flow with an arbitrary inlet temperature and we extend this to calculating fully developed flows in stream-wise periodic passages, specifically in a regular serpentine channel with semi-circular cross-section. Such a flow arrangement is typical of compact heat exchangers where flow and heat transfer occurs in a large number of repeating unit structures or modules. After a sufficient entrance length (number of units), the flow and non-dimensional temperature patterns become invariant from module to module, and can be described as fully developed.

2. Problem specification

We consider the general case of a swept duct of constant cross-section and length S. The duct is created by sweeping its cross-section in a normal plane along a path whose radius of curvature is sufficient to ensure that points on the circumference are also swept smoothly without creating unphysical overlaps. For a circular-section duct of diameter d, for example, the minimum radius of curvature of the swept path at the centre of the section is $R_c > d/2$.

Consider a duct (length S) in which a total rate of heat transfer Q_W occurs. The **H1** and **H2** boundary conditions, as defined by Shah and London [1], require that the so-called axial heat flux is constant along the length:

$$q'(s) = Q_W/S = q'_W \tag{1}$$

The **H1** boundary condition requires that the peripheral wall temperature at a given location s is constant:

$$T|_P = T_W(s,p) = \text{constant} \tag{2}$$

and the axial heat flux ($q'(s)$) is related to the average ($\bar{q''}$) and peripherally local ($q''(s,p)$) wall heat fluxes via

$$q'(s) = \bar{q''} \cdot P = \int_P q''(s,p) w(p)\,\mathrm{d}p \tag{3}$$

where $w(p)$ is the relative dilatation of the channel surface at p due to the curvature of the duct path (it is positive on the outside of the bend and negative on the inside). From Fig. 1, which shows a small segment of channel of length ds, it can be seen that

$$w(p) = \frac{\mathrm{d}s_W(p)}{\mathrm{d}s} = \frac{[R_c + r_W(p)]\mathrm{d}\theta}{R_c \mathrm{d}\theta} = \frac{R_c + r_W(p)}{R_c} \tag{4}$$

where $R_c + r_W(p)$ is the distance of the point on the wall from the sweep axis in the swept plane.

For the **H2** boundary condition, it is a requirement that the local heat flux be uniform around the periphery of the duct:

$$q''(s,p) = -k\left.\frac{\mathrm{d}T}{\mathrm{d}n}\right|_p = \text{constant} \tag{5}$$

A particularly simple specification of q'' arises for a symmetrical cross-section with its line of symmetry aligned parallel to the axis of the sweep and located a distance R_c from that axis. In this case, $r_W(p)$ is an odd function for which

$$\int_P r_W(p)\,\mathrm{d}p = 0 \tag{6}$$

i.e. the expansion of area on one side of the duct is balanced by the reduction of area on the other. This results in

$$\int_P w(p)\,\mathrm{d}p = P \tag{7}$$

and the **H2** boundary condition can be expressed explicitly and is simply given as

$$q''(s,P) = \frac{q'_W}{P} = \frac{Q_W}{S \cdot P} = q''_W \tag{8}$$

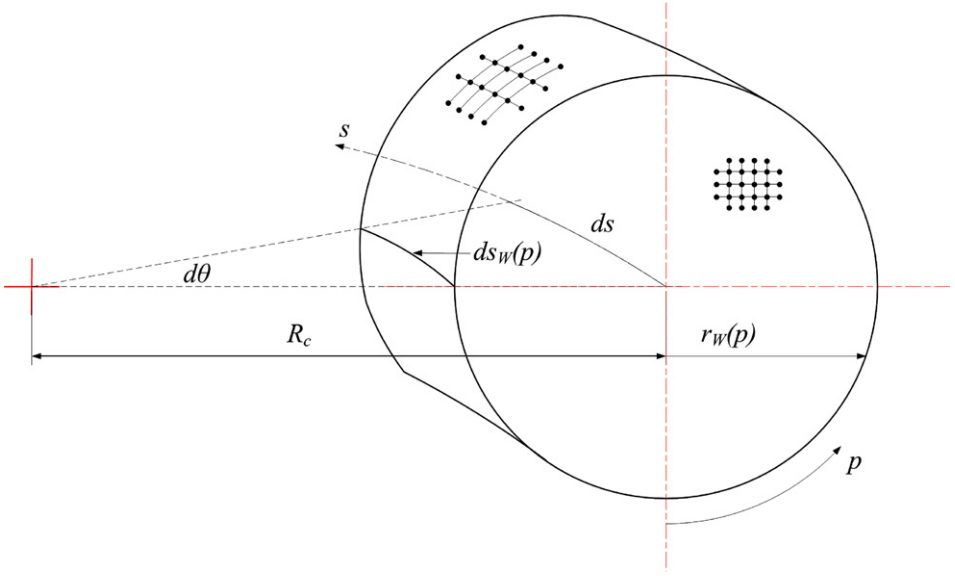

Fig. 1. Duct geometry created by sweeping a constant cross-section (a circular cross-section is pictured) along a given axial path, s.

The **H2** boundary condition is then sufficiently general and trivial to implement in any commercial CFD code.

The situation is more complex for the **H1** boundary condition in non-straight passages, for which the wall temperature at an axial location is constant but not known *a priori*:

$$T_W(s,p) = T_W(s), \quad \text{an unknown function} \tag{9}$$

The local heat flux varies around the periphery of the duct and the requirement of a constant axial heat flux is not simply expressed in terms of a universal boundary condition that is easily available in a commercial CFD code (such as universally constant T_W or q''). The problem, which equates to finding $T_W(s)$ to satisfy the constant axial flux condition, cannot be solved directly. Of course, if the wall temperature distribution is known in advance, it is a standard computation to calculate $q''(s,p)$ and thence $q'(s)$ from Eq. (3) – this suggests an approach to determining $T_W(s)$ iteratively from an initial guess to a final function that satisfies constant axial heat flux. For this, we adopt a Newton–Raphson approach, as described below.

3. Solution methodology

Patankar et al. [18] described a technique for the solution of stream-wise periodic flow and heat transfer problems. Implementation of this technique is generally specific to a given geometry (see, for example, [19]) and the boundary conditions must be written specifically into the solver which, for the **H1** boundary condition, is not generally accessible in commercial CFD codes.

For fluid flow with constant properties, the flow field is independent of the temperature field and the continuity and Navier–Stokes equations may be solved to obtain the velocity field prior to the solution of the energy equation. Computations are carried out using ANSYS CFX-10 [20], a finite-volume CFD code. All calculations are performed using a second-order bounded differencing scheme for the convective terms.

The problem of solving the energy equation to satisfy the **H1** boundary condition is split into two parts. Firstly, we determine the appropriate wall temperature distribution $T_W(s)$ to achieve constant axial wall heat flux $q'(s)$ for a fixed inlet temperature profile – this is the solution to a developing flow problem. We then modify the inlet fluid temperature distribution by scaling and wrapping of the duct exit profile, the converged solution reflecting the solution for fully developed flows with the **H1** boundary condition.

The duct is created by sweeping a constant cross-section along an axial path of arbitrary shape (Fig. 1). Through the use of a swept mesh, nodes (at which calculated values are to be obtained) fall into groups determined by their axial location s. An example of a swept mesh, where the inlet face is extruded along the axial path, s, is shown in Section 4.1. A hexahedral mesh has been used in this case to discretise the model domain in order to maximise computational efficiency and accuracy. The cross-sectional mesh provides greatest resolution in areas containing the highest velocity and temperature gradients, with the mesh being most refined in the vicinity of the walls. The axial mesh is also distributed to provide accurate resolution of the flow throughout the domain.

3.1. Iterative calculation procedure for the *H1* boundary condition

For a given inlet fluid temperature profile (assumed uniform, T_{IN}, in this work), the iterative calculation is initiated by applying an assumed axial distribution of wall temperature. A reasonable first guess is to assume a linear profile with a gradient that is proportional to the axial wall heat flux:

$$T_W - T_{IN} = \frac{q'}{\dot{m}c_p}s \tag{10}$$

The fluid temperature field is determined for the given wall and inlet temperature distribution through the solution of the energy equation using ANSYS CFX-10 [20]. The resulting distribution of wall heat flux per unit length can be calculated using Eq. (3).

In vector notation, we have solved for $\vec{\mathbf{q}}' = [q'_1, q'_2, q'_3, \ldots, q'_N]$ as a function of $\vec{\mathbf{T}} = [T_1, T_2, T_3, \ldots, T_N]$ for each of the axial nodes. We now form the Jacobian matrix

$$[\mathbf{J}] = \begin{bmatrix} \frac{\partial q'_1}{\partial T_1} & \frac{\partial q'_1}{\partial T_2} & \cdots & \frac{\partial q'_1}{\partial T_N} \\ \frac{\partial q'_2}{\partial T_1} & \frac{\partial q'_2}{\partial T_2} & \cdots & \cdots \\ \cdots & & \cdots & \\ \frac{\partial q'_N}{\partial T_1} & \cdots & \cdots & \frac{\partial q'_N}{\partial T_N} \end{bmatrix} \tag{11}$$

by perturbing the wall temperatures, one at a time, at successive downstream locations by a small amount (ΔT_W), repeating the CFD calculation to its new converged solution, and observing the resultant changes in the wall heat flux. Perturbation of the ith temperature allows the ith column of the Jacobian to be populated as $\Delta\vec{\mathbf{q}}'/\Delta T_W$ – for a finely resolved flow-field, this may mean hundreds of CFD iterations just to form the Jacobian and the process is clearly computationally intensive. However, this process lends itself to automation and is straightforward to implement. Fig. 2 shows the results for the perturbation of a node about 10% of the way along a duct discretised as 372 axial nodes. Not surprisingly, the major perturbations in the heat flux distribution occur around the node whose temperature has been perturbed, producing a Jacobian that is diagonally dominant.

For a typical case in which the overall fluid temperature rise in the duct is 10 K $\left(\frac{Q_W}{\dot{m}c_p}\right)$, we find a wall temperature perturbation of 0.5 K provides the best compromise between approximation of the derivatives as ratios of differences and loss of accuracy in off-diagonal (weakly sensitive) terms due to machine precision limitations.

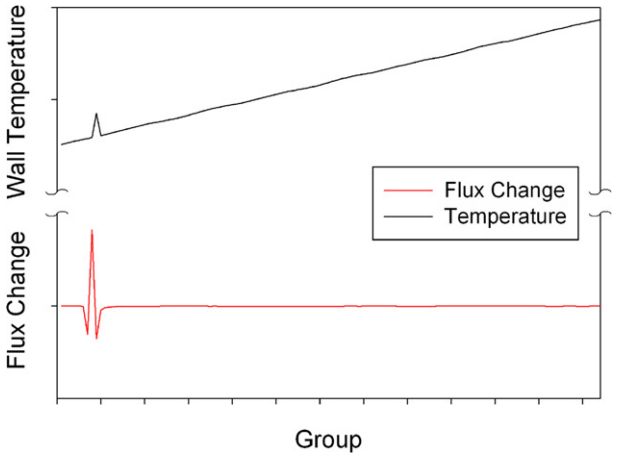

Fig. 2. A schematic of the applied temperature perturbation and resultant change in wall flux (q'). This figure shows a temperature perturbation of $\Delta T_W = 0.5$ K, with the largest flux change approaching $\Delta q'/q' = 0.1$.

Every element of the solution vector $\vec{\mathbf{q}}' = [q'_1, q'_2, q'_3, \ldots, q'_N]$ should ideally equal q'_W but each element is in error by some amount $q'_W - q'_i$, which is represented by the error vector $\boldsymbol{\delta}\vec{\mathbf{q}}'$. Temperature profiles need to be adjusted so that the new solution changes by this amount ($\boldsymbol{\delta}\vec{\mathbf{q}}'$). As the numerical Jacobian is not exact and the overall problem is not linear for large perturbations, we adjust the previous temperature profile by the amount

$$\boldsymbol{\delta}\vec{\mathbf{T}} = f\mathbf{J}^{-1} \cdot \boldsymbol{\delta}\vec{\mathbf{q}}' \tag{12}$$

where f is an under-relaxation factor. Under-relaxation is especially important when a large shift in wall temperature is calculated. We typically start with $f = 0.1$ – the use of a small under-relaxation factor for increased stability does increase the number of iterations required to achieve the desired flux distribution, but the value of the under-relaxation factor can be adjusted (increased) as the run converges.

Jacobian inversion is performed using the LU Decomposition method and back-substitution, utilising the subroutines ***ludcmp*** and ***lubksb*** from Press et al. [21]. We note that the fact that the Jacobian is banded may provide some opportunities for faster methods of inversion but we have not investigated this further here as matrix inversion is a very small cost component of the simulation.

The entire process to implement the **H1** boundary condition for a given inlet temperature profile is shown in the flow diagram of Fig. 3.

3.2. Fully developed flows

Once the **H1** boundary condition has been satisfied for a given inlet temperature profile, we further impose a periodic boundary condition whereby the appropriately scaled outlet temperature is wrapped back to the inlet. The solution of this problem also requires further iterations on the wall temperature profile in order also to satisfy the **H1** boundary condition – we have found that this two-step approach to fully developed **H1** solution is much faster and more robust than attempting to solve in a single step because the wrapping introduces gross perturbations when far from the solution.

Fully developed flow is achieved when the non-dimensional temperature profiles are identical at both the inlet and the outlet of the wrapped section:

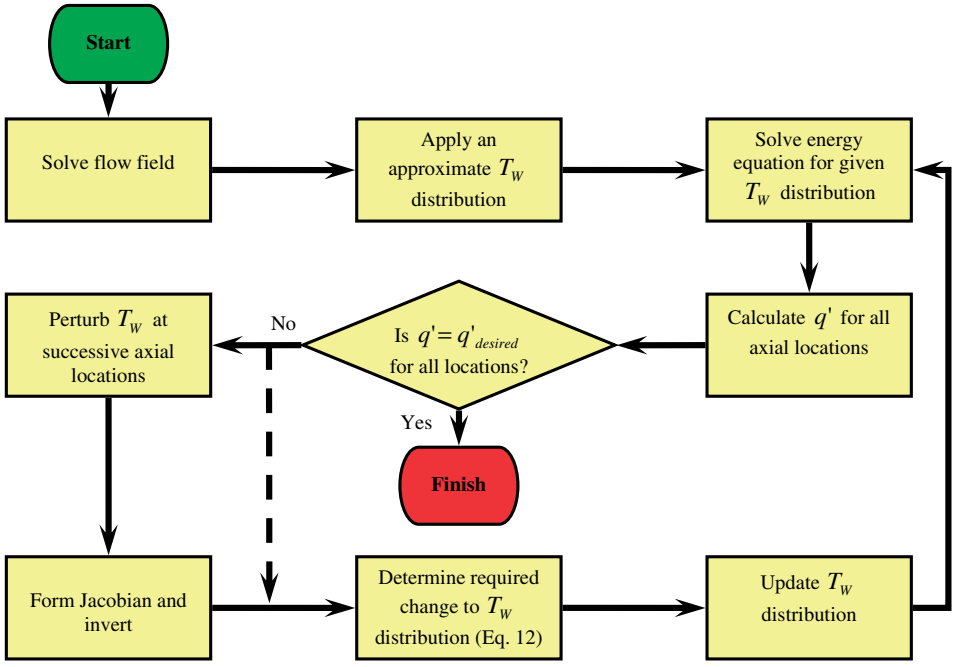

Fig. 3. Flow diagram for the implementation of the **H1** boundary condition for a given inlet temperature profile. The dashed path represents a shortcut in which the Jacobian is evaluated only once and is reused many times (see Sections 3.2 and 4.3).

$$\theta_{\text{in}} = \left(\frac{T_{\text{W}} - T_{x,y}}{T_{\text{W}} - \overline{T}_{\text{B}}}\right)_{\text{in}} = \left(\frac{T_{\text{W}} - T_{x,y}}{T_{\text{W}} - \overline{T}_{\text{B}}}\right)_{\text{out}} = \theta_{\text{out}} \qquad (13)$$

For the **H1** boundary condition, the temperature profiles are identical in shape at the inlet and outlet of the geometry, but are displaced by an amount that is equal to the fluid temperature rise in the unit ($= Q_{\text{W}}/\dot{m}c_p$). This is the same condition as applies for the **H2** condition and we use the same procedure as described in our earlier work [22,23].

The convergence of the wrapped solution brings a new inlet temperature distribution, different from that assumed, and the wall temperatures must again be adjusted as described in the previous section to re-establish the **H1** boundary condition. In general, this calculation is much quicker than obtaining the first **H1** solution with arbitrary inlet fluid temperature profile, and becomes faster with each wrapping. The process is repeated until the fully developed flow in the periodic geometry is achieved and the **H1** boundary condition is satisfied.

The procedure for simulating fully developed laminar flow and heat transfer behaviour in periodic non-straight passages subject to the **H1** boundary condition is computationally expensive, given the large number of axial locations where the wall temperature is specified. The most computationally intensive component of the simulation is the formation the Jacobian matrix, as a converged temperature solution must be obtained for wall temperature perturbation of each of the N axial locations. One method of reducing computational cost is to reuse the Jacobian for several temperature updates (with this procedure shown via the dotted line in the flow diagram of Fig. 3). This has the advantage of reducing the total number of computational steps required; however, the Jacobian may become outdated and no longer approximate the change in wall heat flux accurately for the given change in wall temperature (ΔT_{W}), thus decreasing stability and accuracy. This is problem specific, and the effect of using this approach is discussed for the serpentine channel with semi-circular cross-section in Section 4.3.

3.3. Validation

We have validated the method against results published in Shah [24] for the local Nusselt number found in hydrodynamically developed and thermally developing flow in straight ducts of both circular and semi-circular cross-sections. As shown in Fig. 4, our computations for the circular-section agree within 0.3% of the data taken from Shah [24] for $x^* > 0.002$. For $x^* < 0.002$, a loss of precision (1.9% at $x^* = 0.001$) relates to both the increasing dominance of axial conduction and the length scale of the axial discretisation employed in the near-entrance region of the duct, and not to any intrinsic problem with the method. Since, in general, Nu varies as $x^{*-1/3}$ as $x^* \to 0$, there is theoretically no limit to the grid refinement needed to get an accurate result as x^* decreases – it is simply a question of refining the axial grid to the point that the minimum value of x^* to be considered is axially resolved.

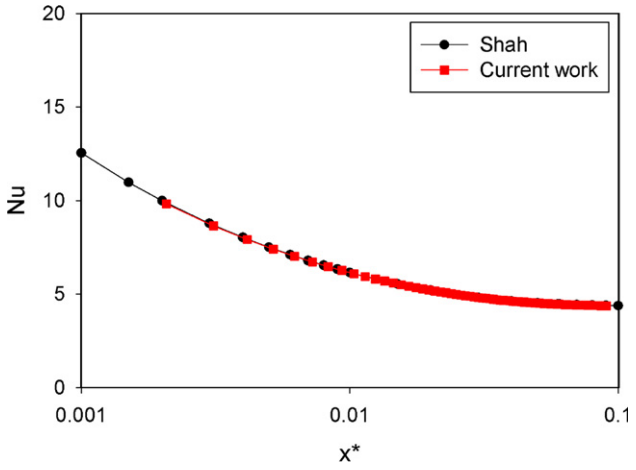

Fig. 4. Local Nu as a function of x^* $(\frac{x}{d_h Pe})$ for thermally developing and hydrodynamically developed flow in a duct with circular cross-section.

Results for ducts with a semi-circular cross-section (Fig. 5) show good agreement with data found in Lei and Trupp [12]. Errors larger than 3% are found for $x^* \leqslant 0.003$, however, this loss of precision is again attributed to the length scale of the axial discretisation employed in the region closest to the entrance of the duct.

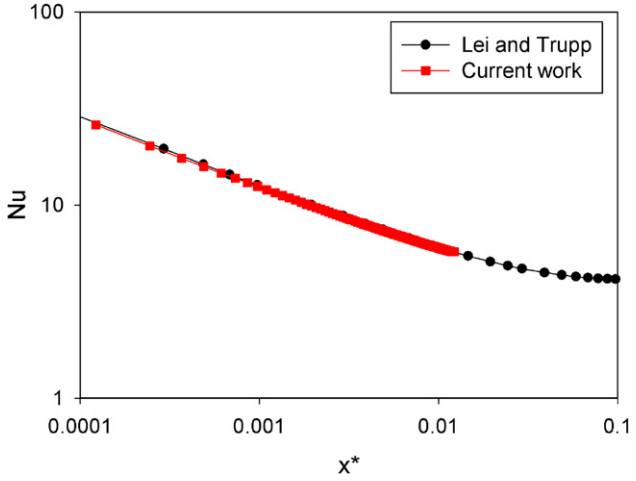

Fig. 5. Local Nu as a function of x^* $(\frac{x}{d_h Pe})$ for thermally developing and hydrodynamically developed flow in a duct with semi-circular cross-section.

Table 2
Nusselt numbers for fully developed flow in straight ducts of various cross-sections

Cross-section	Nu_{H1} (Current results)	Nu_{H1} [1]	Difference (%)
Circular	4.366	4.364	0.046
Square	3.615	3.608	0.202
Semi-circular	4.090	4.089	0.024

Values are compared with those found in Shah and London [1] for validation.

Validation of our calculations is also provided by comparison of Nusselt numbers for fully developed flow and heat transfer ($x^* \to \infty$) with analytical solutions [1] for ducts with circular, semi-circular and square cross-sections. As shown in Table 2, the maximum deviation is 0.2%.

4. Fully developed heat transfer in serpentine channels – H1 boundary condition

We have previously reported a study of the fully developed thermohydraulic performance of serpentine channels subject to the **H2** and **T** boundary conditions [23]. We now extend this work to the **H1** boundary condition using the method described above.

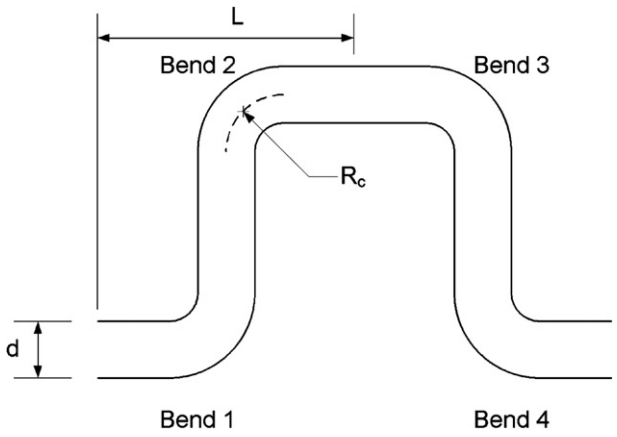

Fig. 6. Schematic of a repeating module of the serpentine geometry showing its axial shape. The non-dimensional geometrical parameters of interest are L/d and R_c/d.

Serpentine channels are defined by sweeping a semi-circle along a serpentine path with the flat face of the semi-circle being in the swept plane, and are fully characterised by the serpentine wavelength ($2L$), channel diameter (d) and the radius of curvature (R_c) of the bend (Fig. 6). Dimensional similitude is achieved via the ratios L/d and R_c/d. The hydraulic diameter, on which both the Reynolds and Nusselt numbers are based, is given by

$$d_h = \frac{\pi}{\pi + 2} d \tag{14}$$

Here we consider fully developed flow, for $L/d = 4.5$, $R_c/d = 1$ and $Pr = 6.13$.

4.1. Model discretisation

Grid independence tests have been carried out in the previous study Rosaguti et al. [23]. The mesh used contains approximately 2100 elements on the inlet cross-section, Fig. 7a, with the repeating unit having more than 245,000 volume elements (Fig. 7b). This equates to 124 axial groups at which the wall temperature must be adjusted in order to satisfy the **H1** boundary condition.

4.2. Results

The results for the fluid flow field are identical to those reported previously [23]. The serpentine passage gives rise to strong secondary flow effects in the form of Dean vortices in the vicinity of the bends in the system. These in turn give rise to substantial variations in the peripherally averaged heat transfer coefficient along the length of the duct.

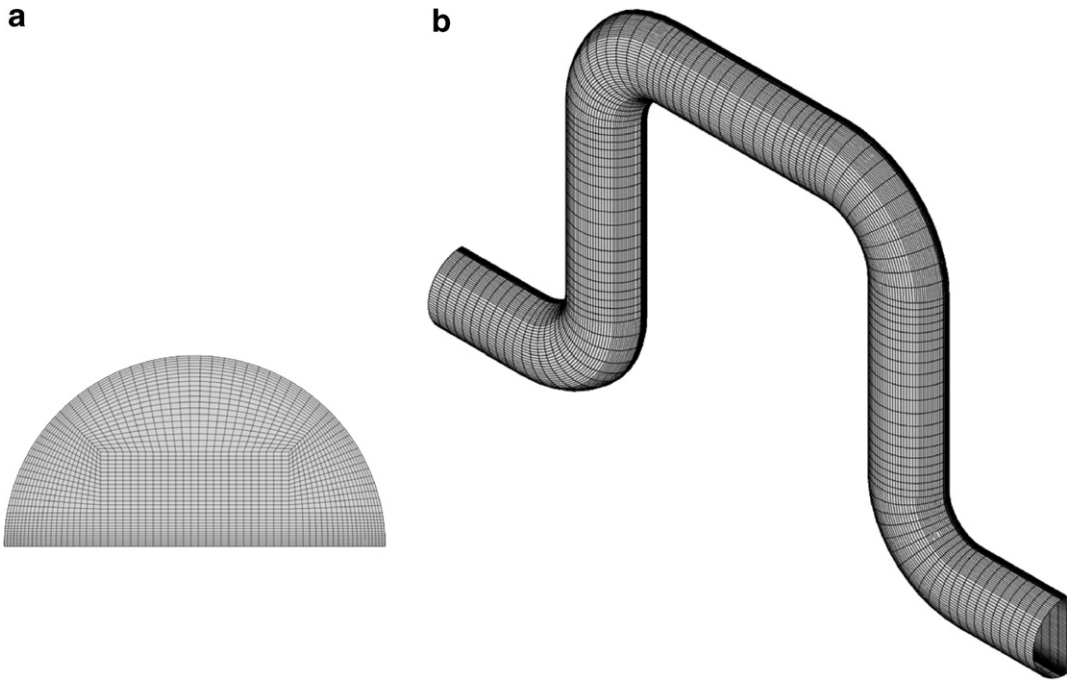

Fig. 7. Mesh density (a) on a cross-section and (b) along the axial direction.

Typical non-dimensional temperature profiles are shown in Fig. 8 for the **H1**, **H2** and **T** boundary conditions at the inlet of the geometry. In all cases, hot fluid is transported by secondary flows away from the hot walls into the centre of the cross-section. However, there are significant differences in the fluid temperature distributions obtained for the different boundary conditions: for **H1**, there is reduced heat transfer in the corners of the cross-section, a result both of the thermal boundary condition and of the low velocities there. For **H2**, the fixed energy flux at every point on the perimeter causes local hot-spots in the corners of the cross-section and in regions of slow moving fluid. The absence of hot spots for the **H1** and **T** boundary conditions leads to similar non-dimensional temperature contours.

An interesting feature of the solution with the **H1** boundary condition in these channels is the fact that the wall temperature does not increase monotonically with axial distance. The wall temperature profile along the length of the channel is shown in Fig. 9 for a range of Reynolds numbers. The reduction in wall temperature corresponds to the increase in the rate of heat transfer at bends, and occurs because a constant axial heat flux per unit length is maintained. After the bends, there is an increase in wall temperature as flow redevelopment occurs in the straight sections of pipe and the rate of heat transfer decreases.

Finally, Fig. 10 shows a comparison of the average Nusselt number in the serpentine duct relative to its value under the same boundary conditions in a straight semi-circular duct – see Table 1 for the three boundary conditions **H1**, **H2** and **T**. As previously reported for the **H2** and **T** boundary conditions [22,23] there is a strong effect of flow Reynolds numbers on the extent of heat transfer enhancement. However, the enhancement of the Nusselt number depends only weakly on the thermal boundary condition, with the **H1** boundary condition giving slightly less

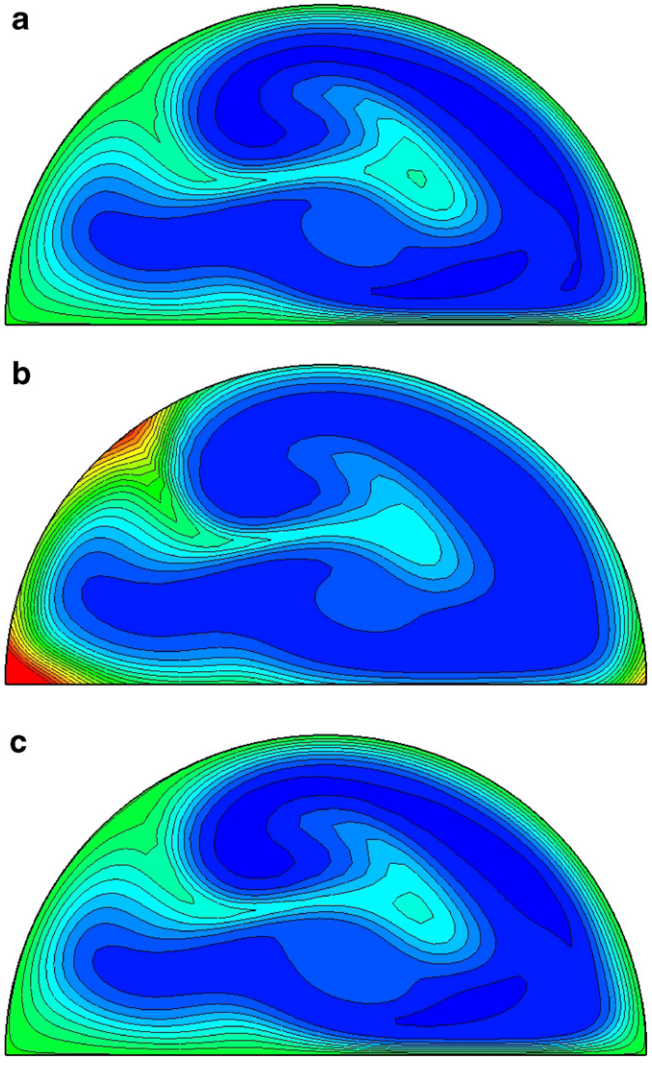

Fig. 8. Non-dimensional temperature contours at the inlet for (a) **H1**, (b) **H2** and (c) **T** boundary conditions for $L/d = 4.5$, $R_c/d = 1$ and a Reynolds numbers of 400. The colours red and blue indicate regions of hot and cold fluid, respectively. (For interpretation of the references in colour in this figure legend, the reader is referred to the web version of this article.)

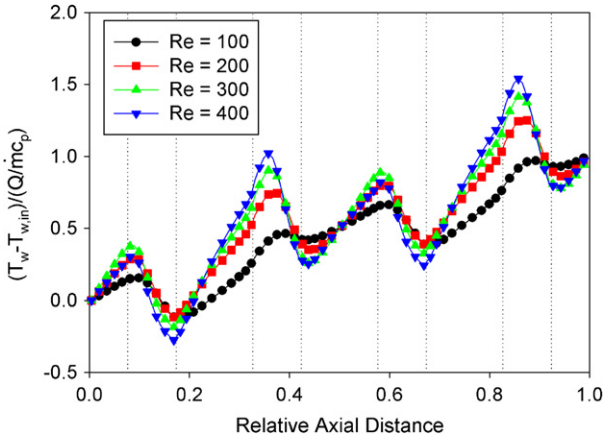

Fig. 9. Normalised wall temperature distributions as a function of position within a serpentine unit for $L/d = 4.5$, $R_c/d = 1$ and Reynolds numbers of: 100, 200, 300 and 400 for the **H1** boundary condition. Dashed lines indicate the relative position of the bends.

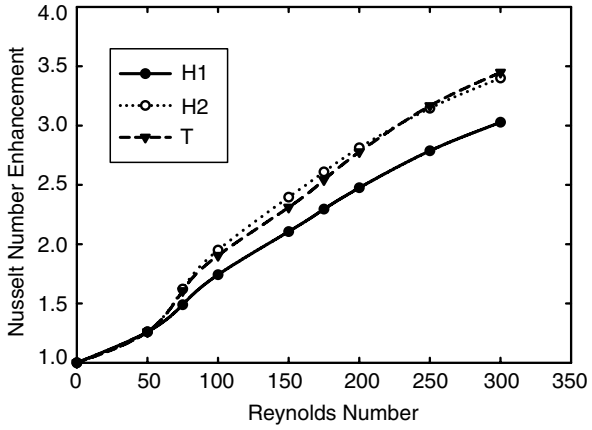

Fig. 10. Comparison of section-average heat transfer enhancement relative to flow in straight semi-circular ducts for fully developed flows with the **H1**, **H2** and **T** boundary conditions.

enhancement than the **H2** and **T** conditions for which the section-average results are essentially indistinguishable.

4.3. Computational costs

As mentioned in Section 3.1, the procedure for simulating fully developed laminar flow and heat transfer behaviour in non-straight passages subject to the **H1** boundary condition is computationally expensive. The major portion of this cost is incurred in repeated evaluations of the Jacobian – this is shown in Fig. 10 which shows the progress of convergence to the **H1** solution (for developing flow in the serpentine passage) in terms of the total number of CFD iterations, with the spacing between the black circular symbols representing the number of iterations needed to form each new Jacobian. We have investigated the reuse of the Jacobian matrix as a method to reduce the overall computational cost, as depicted schematically by the dashed line in Fig. 3. Whereas continual updating of the Jacobian requires approximately 4000 CFD iterations to achieve a limiting residual of $|\delta q'|/q' \sim 10^{-5}$, the reuse of the first Jacobian achieves the same level of convergence in less than 1000 CFD iterations, as shown in Fig. 11.

To obtain results for a single case of fully developed flow within periodic serpentine channels with semi-circular cross-section using the means of computational cost saving mentioned above, simulations for the **H1** boundary condition take more than 25 times longer than those for the **H2** or **T** boundary conditions, solving only the energy equation. For reference, simulations for the **H1** boundary condition take approximately a day to complete on a PC with 3 GHz CPU and 2GB RAM. Typical relaxation factors used in these computations ranged from 0.1 at the very start of a run (required when a large temperature change is necessary) to 1 as the run converges. Due to reuse of the Jacobian, use of a small relaxation factor does not greatly increase computational cost.

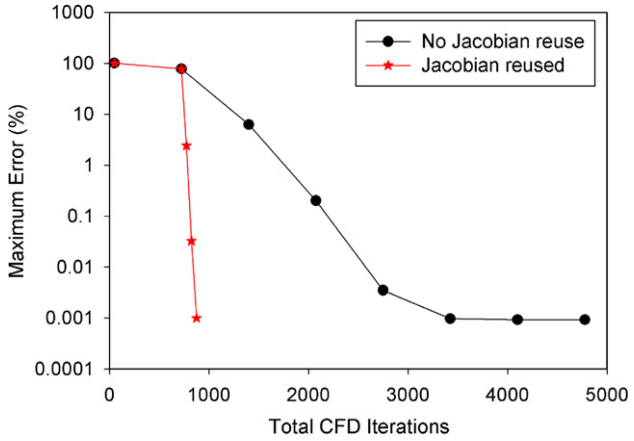

Fig. 11. Test results for Jacobian reuse, showing the maximum error $\left(\mathrm{Max}\left(\left|\frac{q'-q'_{\mathrm{desired}}}{q'_{\mathrm{desired}}}\right|_s\right)\right)$ in the wall heat flux for 5000 CFD iterations. The data set with circular symbols use a new Jacobian for each wall temperature update.

5. Conclusions

The case of constant axial wall heat flux with constant peripheral wall temperature (the **H1** thermal boundary condition) provides a more physically representative thermal boundary condition for simulating heat exchangers with finite peripheral wall conduction, accounting in a first-order manner for the role of the substrate material surrounding the duct. Simulations using the **H1** boundary condition to understand the effects of channel shape and pathway are therefore of great utility in the design of heat transfer equipment. This boundary condition is not available in commercial CFD software and is not straightforward to implement. For this reason, a methodology has been developed to implement the **H1** thermal boundary condition in a CFD code that allows heat transfer simulations in non-straight passages for steady, laminar, incompressible, single-phase flow of a Newtonian fluid with constant physical properties.

Validation cases for developing and fully developed flow in straight ducts have shown the implemented method to be very accurate. Fully developed laminar flow and heat transfer behaviour in periodic serpentine channels with a semi-circular cross-section subject to the **H1** boundary condition has been investigated as an example of a typical channel geometry. Results have been presented for the geometric configuration where $R_c/d = 1$, $L/d = 4.5$, for Reynolds numbers up to 400 and fluids with a Prandtl number of 6.13. A non-monotonic temperature distribution along the duct is seen to exist in order to maintain a constant axial heat flux per unit length due to increased rates of heat transfer through bends. This temperature gradient is shown to be strongly dependent on the Reynolds number and position with respect to bends in the duct.

The effect of the thermal boundary condition on the non-dimensional temperature distribution has been compared for the **H2**, **T** and **H1** boundary conditions, utilising previous work by the current authors. Results indicate that hot spots within the passage cross-section, typical of the **H2** boundary condition, are removed in the **H1** case.

The methodology described to study the **H1** boundary condition in non-straight passages incurs a large computational cost, significantly greater than that required to study the **H2** or **T** boundary conditions. This is because of the need to construct a Jacobian matrix that relates changes of wall temperatures to wall heat fluxes. Computational costs, however, can be minimised through reuse of the Jacobian matrix used to update the wall temperatures. Tests indicate that for fully developed flow in a periodic serpentine passage with a given inlet temperature, the creation of a single Jacobian is sufficient to achieve a constant axial wall heat flux distribution.

Acknowledgements

The authors acknowledge the support of Heatric and the Australian Research Council for an APAI scholarship for

Nathan Rosaguti. This work is supported by Heatric/Meggitt PLC.

References

[1] R.K. Shah, A.L. London, in: T.F. Irvine, J.P. Hartnett (Eds.), Advances in Heat Transfer, Supplement 1, Laminar Flow Forced Convection in Ducts, Academic Press, New York, 1978.
[2] J.M. Choi, N.K. Anand, Heat-transfer in a serpentine channel with a series of right-angle turns, Numer. Heat Transfer, Part A – Appl. 23 (1993) 189–210.
[3] S. Chintada, K.H. Ko, N.K. Anand, Heat transfer in 3-D serpentine channels with right-angle turns, Numer. Heat Transfer, Part A – Appl. 36 (1999) 781–806.
[4] G. Comini, G. Croce, Convective heat and mass transfer in tube-fin exchangers under dehumidifying conditions, Numer. Heat Transfer, Part A – Appl. 40 (2001) 579–599.
[5] G. Comini, C. Nonino, S. Savino, Effect of aspect ratio on convection enhancement in wavy channels, Numer. Heat Transfer, Part A – Appl. 44 (2003) 21–37.
[6] S. Savino, G. Comini, C. Nonino, Three-dimensional analysis of convection in two-dimensional wavy channels, Numer. Heat Transfer, Part A – Appl. 46 (2004) 869–890.
[7] Haitham M.S. Bahaidarah, N.K. Anand, Numerical study of heat and momentum transfer in channels with wavy walls, Numer. Heat Transfer, Part A – Appl. 47 (2005) 417–439.
[8] Y. Chen, M. Fiebig, N.K. Mitra, Conjugate heat transfer of a finned oval tube part A: flow patterns, Numer. Heat Transfer, Part A – Appl. 33 (1998) 371–385.
[9] R.K. Shah, Fully developed laminar flow forced convection in channels, in: S. Kakac, R.K. Shah, A.E. Bergles (Eds.), Low Reynolds Number Flow Heat Exchangers, Hemisphere Publishing Corporation, Washington, 1983, pp. 75–108.
[10] G.L. Morini, Analytical determination of the temperature distribution and Nusselt Numbers in rectangular ducts with constant axial heat flux, Int. J. Heat Mass Transfer 43 (2000) 741–755.
[11] L. Ghodoossi, N. Eğrican, Prediction of heat transfer characteristics in rectangular microchannels for slip flow regime and H1 boundary condition, Int. J. Thermal Sci. 44 (2005) 513–520.
[12] Q.M. Lei, A.C. Trupp, Forced convection of thermally developing laminar flow in circular sector ducts, Int. J. Heat Mass Transfer 33 (8) (1990) 1675–1683.
[13] R.M. Manglik, P.P. Fang, Effect of eccentricity and thermal boundary conditions on laminar fully developed flow in annular ducts, Int. J. Heat Fluid Flow 16 (1995) 298–306.
[14] R. Sadasivam, R.M. Manglik, A.J. Milind, Fully developed forced convection through trapezoidal and hexagonal ducts, Int. J. Heat Mass Transfer 42 (1999) 4321–4331.
[15] R.K. Shah, S.D. Joshi, Convective heat transfer in curved ducts, in: S. Kakac, R.K. Shah, W. Aung (Eds.), Handbook of Single-Phase Convective Heat Transfer, John Wiley & Sons, New York, 1987.
[16] C.E. Kalb, J.D. Seader, Heat and mass transfer phenomena for viscous flow in curved circular tubes, Int. J. Heat Mass Transfer 15 (4) (1972) 801–817.
[17] C.J. Bolinder, B. Sundén, Numerical prediction of laminar flow and forced convective heat transfer in a helical square duct with a finite pitch, Int. J. Heat Mass Transfer 39 (15) (1996) 3101–3115.
[18] S.V. Patankar, C.H. Liu, E.M. Sparrow, Fully developed flow and heat transfer in ducts having streamwise-periodic variations of cross-sectional area, J. Heat Transfer 99 (1977) 180–186.
[19] R.M. Manglik, J. Zhang, A. Muley, Low Reynolds number forced convection in three-dimensional wavy-plate-fin compact channels: fin density effects, Int. J. Heat Mass Transfer 48 (8) (2005) 1439–1449.
[20] ANSYS, CFX Computational Fluid Dynamics (CFD) software, 2005. <http://www.ansys.com/cfx>.
[21] W.H. Press, S.A. Teukolsky, W.T. Vetterling, B.P. Flannery, Numerical Recipes in Fortran, second ed., Cambridge University Press, New York, 1992.
[22] N.R. Rosaguti, D.F. Fletcher, B.S. Haynes, Laminar flow and heat transfer in a periodic serpentine channel, Chem. Eng. Technol. 28 (3) (2005) 353–361.
[23] N.R. Rosaguti, D.F. Fletcher, B.S. Haynes, Laminar flow and heat transfer in a periodic serpentine channel with semi-circular cross-section, Int. J. Heat Mass Transfer 49 (17–18) (2006) 2912–2923.
[24] R.K. Shah, Thermal entry length solutions for the circular tube and parallel plates, in: Proceedings of the 3rd National Heat and Mass Transfer Conference, Indian Institute of Technology, Bombay, India, Paper No. HMT-11-75, 1975.